# Non-Brownian dynamics and strategy of amoeboid cell locomotion

Shin I. Nishimura*
*Department of Mathematical and Life Sciences, Hiroshima University, Hiroshima 739-8526, Japan*

Masahiro Ueda
*Laboratories for Nanobiology, Graduate School of Frontier Biosciences, Osaka University, Suita, Osaka 565-0871, Japan, JST, CREST, Suita, Osaka 565-0871, Japan, and Quantitative Biology Center (QBiC), RIKEN, OLABB, Furuedai 6-2-3, Suita, Osaka 565-0874, Japan*

Masaki Sasai
*Department of Computational Science and Engineering, Nagoya University, Nagoya 464-8603, Japan, School of Computational Sciences, Korea Institute for Advanced Study and Okazaki Institute for Integrative Bioscience, Okazaki 444-8787, Japan*

(Received 26 October 2011; published 11 April 2012)

Amoeboid cells such as *Dictyostelium discoideum* and Madin-Darby canine kidney cells show the non-Brownian dynamics of migration characterized by the superdiffusive increase of mean-squared displacement. In order to elucidate the physical mechanism of this non-Brownian dynamics, a computational model is developed which highlights a group of inhibitory molecules for actin polymerization. Based on this model, we propose a hypothesis that inhibitory molecules are sent backward in the moving cell to accumulate at the rear of cell. The accumulated inhibitory molecules at the rear further promote cell locomotion to form a slow positive feedback loop of the whole-cell scale. The persistent straightforward migration is stabilized with this feedback mechanism, but the fluctuation in the distribution of inhibitory molecules and the cell shape deformation concurrently interrupt the persistent motion to turn the cell into a new direction. A sequence of switching behaviors between persistent motions and random turns gives rise to the superdiffusive migration in the absence of the external guidance signal. In the complex environment with obstacles, this combined process of persistent motions and random turns drives the simulated amoebae to solve the maze problem in a highly efficient way, which suggests the biological advantage for cells to bear the non-Brownian dynamics.

DOI: 10.1103/PhysRevE.85.041909 PACS number(s): 87.17.Jj, 87.17.Aa

## I. INTRODUCTION

Cell migration plays crucial roles in many processes including neuronal patterning, wound healing, and embryogenesis. Biochemical and cell-biological experiments have revealed that there is a common mechanism underlying cells in those physiological processes and other motile cells such as *Dictyostelium discoideum* amoeba and fish epidermal keratocytes: The branched network of filamentous actin are nucleated at the front of moving cell, which gives rise to the effective pressure to protrude the leading edge forward [1–3]. Investigations of motile cells have further shown that this nucleation for actin polymerization induces the retrograde flow of cortex actin [4,5], and the actin filaments are disassembled at the rear to retract the rear edge of cell [5,6]. One of the important problems, therefore, is to understand how this retrograde flow of cortical actin regulates statistical features of migration [6,7].

Anomalous statistical features of migration have been reported recently for amoeboid cells such as Madin-Darby canine kidney (MDCK) cells [8] and *D. discoideum* [9]: When there is no external cue to guide cells, cells move spontaneously in random directions. Their trajectories, however, do not obey simple Brownian dynamics but are characterized by the superdiffusive increase of the mean-squared displacement (MSD) for the time durations observed in experiments. Though some phenomenological equations of motion have been proposed to fit the observed data [8–10], the physical mechanism of this non-Brownian dynamics has remained totally elusive. Furthermore, the biological advantage for cells to exhibit such superdiffusive movement is not known [8]. In this paper we explain the physical origin of the non-Brownian dynamics by using a theoretical model which focuses on the effects of the retrograde flow of cortical actin and the associated whole-cell scale dynamics. We also show that the mechanism which explains the non-Brownian dynamics can efficiently drive cells in complex environment, suggesting the biological significance of this non-Brownian dynamics.

A number of theoretical models have been developed to explain eukaryotic cell locomotion by simulating dependencies of cell shape on the force-velocity relations [11–13], or by focusing on cell polarization and chemotactic responses [14–22]. In particular, the modified versions of the local-excitation-global-inhibition (LEGI) models have explained random and spontaneous formation of active membrane patches which should enhance protrusion of pseudopodia [16,18,21,22]. Though the appearance and disappearance of such active patches should be important for the fluctuating motion of amoeboid cells, these models could not explain the observed stable polarity which causes cells to turn. It was suggested, therefore, that a slow positive feedback loop which was not taken into account in the LEGI models may be responsible for the long-time behaviors of motile cells [16].

*shin@hiroshima-u.ac.jp

 

In this paper we explore such slow positive feedback loop to explain the non-Brownian movement, which consists of multiple turns and multiple times of cell shape deformation. For investigating such long-time behaviors, we develop a coarse-grained model of migration, which only implicitly takes account of the force-velocity relations and the biochemical signaling pathways but highlights the slow positive feedback effect arising from the retrograde flow of cortex actin in moving cells [23–25].

A key assumption in the model is that molecules which interact with cortex actin should move in conjunction with the retrograde flow, and hence they are sent backward as the cell moves forward. This assumption is consistent with the observations that the fluorescent markers interacting with the cortex actin are conveyed to the rear as the cortex actin is sent backward [5,6]. At the rear of cell, actin filaments are bundled with various actin-binding proteins (ABPs) such as filamin [26,27], cortexillins [28], and others and the bundled actin interacts with myosin II to generate the mechanical force for tail contraction. Nucleation of new actin filaments is suppressed in such bundled actin, so that those ABPs and myosin II effectively inhibit actin polymerization. The bundled actin itself, which is differently organized from the branched network in the leading front, could also be regarded as an inhibitory factor for actin polymerization. It is also possible to imagine that the signaling molecules such as PTEN [29,30] and $PIP_2$ may interact with ABPs and move in a correlated way with the cortex actin. These inhibitory molecules, including ABPs, myosin II, and the bundled actin itself, are conveyed by the flow of cortex actin and should be accumulated at the rear of cell. Since dynamics of distributions of these inhibitory molecules is largely determined by the flow of cortex actin, we here do not specify the precise molecular species, but treat them as a group which is referred to as cortical factor (CF) in the model.

Though individual ABPs can be recruited at the front for some specific work to bundle the actin filaments there, we here highlight the general tendency that CF is sent backward as the cell moves forward. Our assumption on the predominance of the backward flow in dynamics of CF can be naturally implemented in the model if we use a coordinate fixed to the substrate: CF only slowly diffuses in the substrate-fixed coordinate, which implies the existence of a distinct backward flow of CF if we describe it in the coordinate fixed on the moving cell. We here note that the retrograde flow is determined by multiple factors including actin network polymerization, cell adhesion to the substrate [31,32], and cell shape deformation [33], so that the flow is not completely described by the difference between cell-fixed and substrate-fixed coordinates. Indeed, the actin flow shows advection in the substrate-fixed frame [33], and the flow is modulated by the effects of force-generating molecules such as myosins [34,35]. Those residual flows, however, are about 10 times slower than the rate of the leading-edge growth or the motion of the centroid [36,37] in keratocyte or *Dictyostelium*, so that we can neglect their effects as a first approximation by representing the retrograde flow with the difference between two coordinates. Using this trick of modeling the retrograde flow, the simulated CF accumulates at the rear as illustrated in Fig. 1.

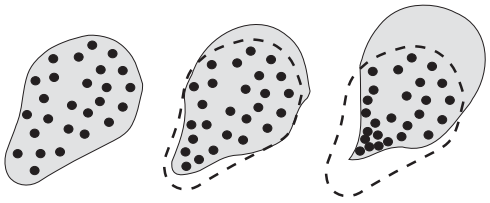

FIG. 1. Schematic illustration of the retrograde flow of cortical factor (CF) in a cell. Black filled circles represent CF. The cell moves upward from left to right, in which the initial position of the cell is indicated by dashed lines. First, CF uniformly distributes (left). As the cell moves, the retraction concentrates CF at the rear, and the protrusion dilutes CF at the front, so that migration induces the retrograde flow of CF in a cell (middle). The polarized distribution of CF further promotes migration (right).

With CF thus defined, we simulate actin polymerization by assuming that actin filaments are nucleated only at the position in the cell where the concentration of CF is below a certain threshold, which implicitly represents the switchlike dynamical competition between excitatory and inhibitory pathways [15,20,38], and we further assume that the increased concentration of the actin network leads to the protrusion of that part of cell while the other parts of cell are retracted to keep the constraint of the approximately constant cell volume [7]; the latter two rules of cell shape deformation represent the implicit force-velocity relations in cells.

With these assumptions, we can show that CF accumulates at the rear when the cell moves forward. The accumulated CF inhibits actin polymerization at the rear, and the diluted CF at the front enhances the protrusion of pseudopodia. Thus, the cell movement generates the CF polarity, and the CF polarization further enhances the cell movement. In this way, the CF distribution and cell movement form a slow positive feedback loop, which we call the CF feedback. In this paper we show that this positive feedback can generate switchlike behaviors between two states: In one state, which we call the persistent state, the straightforward motion is stabilized through the polarized CF, and in the other state, which we call the turning state, the cell shape deformation decreases the CF polarity, and the decreased CF polarity enhances cell deformation and erases the memory of the previous persistent motion to turn the cell into a new direction.

In the following, we first explain that the model can generate different modes of cell migration, which will be used to clarify the dynamical features of migration examined in this paper. We then show that the switchlike dynamics underlies the superdiffusive motion of *Dictyostelium*, and we show that the same dynamical features facilitate the efficient route-finding behaviors of the simulated amoeboid cell in a mazelike complex environment.

## II. RESULTS

### A. Amoeba- and keratocyte-like migration

In order to examine the cell movement quantitatively, it is useful to compare different modes of migration by analyzing how such difference is reflected in important quantities. We first show that both two modes of migration, the amoeba-like migration with protruding pseudopodia to move in a

fluctuating way and the keratocyte-like migration which shows the half-moon cell shape to move in a straightforward way, can be simulated with the present model. For that purpose, we begin with a brief sketch of the model by leaving its detailed definition and explanation of parameters to Supporting Material and Table S1 [39].

To simulate a crawling cell on a substratum, the cell is modeled on a two-dimensional plane that consists of discrete hexagonal sites. Here the hexagonal lattice is adopted to prevent the anisotropic effects arising from the lattice discreteness: If we would use the square lattice, the simulated overall shape of cell body tends to be square. This artifact can be removed if we use the hexagonal lattice, which has the higher symmetry than the square lattice. A cell is defined by a set of connected sites in the hexagonal lattice, which we call "cortical sites." Other noncellular sites are "external sites." See Fig. S1 in Supporting Material [39] for the illustration of the model plane. We assume that a typical cell consists of the moderate number of 900 cortical sites to avoid both the numerical inefficiency to calculate a cell having too large size and the unwanted effects of the lattice discreteness in a cell having too small a size.

Each cortical site has three chemical species; the branched network of filamentous actin, CF, and the signal chemoattractant, whose local concentrations at the $j$th site are $F_j$, $C_j$, and $S_j$, respectively. In external sites, only $S_j$ can be nonzero. $C_j$ and $F_j$ are dynamical variables within a cell, which are updated at each simulation step by following the rules explained in Supporting Material [39]: $C_j$ is changed through the slow diffusion to the adjacent cortical site, which simulates the effective retrograde flow that becomes visible when we describe it in the moving cell-fixed coordinate. $F_j$ does not diffuse to accommodate the retrograde flow in the cell-fixed coordinate but is decreased through disassembly to monomers or transformation to the bundled filamentous form and is increased through actin polymerization. These processes of $F_j$ and $C_j$ are simulated by updating them at each step to $F_j'$ and $C_j'$, respectively, as

$$F_j' = F_j + \begin{cases} \gamma - k_f F_j \ (\text{if } C_j < \alpha(S_j),\ j \in \text{periphery}), \\ -k_f F_j \ (\text{otherwise}), \end{cases} \quad (1)$$

$$C_j' = C_j + \beta(S_j) - k_\beta C_j. \quad (2)$$

In Eq. (1), the actin polymerization with the rate $\gamma$ is considered only at the cell periphery, but degradation with the rate $-k_f F_j$ takes place at every cortical site. In Eq. (2), $\beta$ is the rate of transferring CF from cytosol to cortical layer and $k_\beta$ is the rate constant of the reverse process. Here we assumed that the initiation of actin network formation is cooperative due to the local feedback effects in regulating actin polymerization [38] and hence should nonlinearly depend on $C_j$. In the model this nonlinearity is represented by the rule that $F_j$ increases with the rate $\gamma$ only when $C_j$ is smaller than a threshold $\alpha(S_j)$. Kinetics of actin polymerization is, therefore, controlled by $\alpha(S_j)$ and $\gamma/k_f$.

Effects of the chemical signal are represented in the model through how $\alpha$ and $\beta$ depend on $S_j$. As has been assumed in the LEGI models [15,16], it is natural to assume that the signal molecules enhance both the local excitation and the global inhibition: Here the local excitation is represented by increase in $\alpha(S_j)$, and CF behaves as a signal-dependent global inhibitor which can diffuse over the cell. Signal molecules bound to the receptors near the site $j$ should promote initiation of actin polymerization there, so that $\alpha(S_j)$ should be an increasing function of $S_j$. When receptors are unsaturated, $\alpha(S_j)$ can be a linear function of $S_j$ as $\alpha(S_j) = \alpha_0(1 + aS_j)$ with a constant $a > 0$. Signal molecules should also promote transfer of CF from cytosol to membrane, so that we assume $\beta(S_j) = \beta_0(1 + bS_j)$ with a constant $b > 0$. When enhancement of the local excitation and enhancement of the global inhibition arise from the common upstream signaling process, we may be able to assume $a \approx b$. In this case we have $\beta(S_j)/\alpha(S_j) \approx \beta_0/\alpha_0$ for the uniform signal level with $S_j =$ constant. Then the actin polymerization and hence the cell motion are not altered much by a uniform increase of the signal, so that the simulated cell should show "adaptation" to such uniform increase of the signal as has been observed in experiments [40].

In this model, cell is assumed not to slide on the substratum, but it proceeds by creating new adhesive bonds at the front and detaching from the substratum at the rear, which is simulated as creation of new cortical sites at the front and annihilation of cortical sites at the rear. Creation of new cortical sites is driven by the development of actin network, which is simulated by turning an external site to a new cortical site when the nearby cortical site has $F_j$ larger than a threshold $F_{\text{th}}$. To keep the cell volume approximately constant, a cortical site at the periphery of cell is randomly selected, and the site is turned into the external site, which simulates the retraction of cell body. In this way, chemical reactions, diffusion of CF, and the cell shape deformation are simulated simultaneously.

By fixing $k_f$, $k_\beta$, $\beta_0$, $a$, and $b$ as explained in the Supporting Material [39], we explore the different kinetics of actin polymerization by varying the remaining parameters $\alpha_0$ and $\gamma$: With the larger $\alpha_0$, actin polymerization is triggered at the wider region of the cell, and with the larger $\gamma$, actin polymerization is more rapid. Various different modes of motion are realized by changing $\alpha_0$ and $\gamma$. For example, for small $\alpha_0$ and large $\gamma$, cell is amoeba-like [Fig. 2(a) and Movie S1 [39]], and for large $\alpha_0$ and small $\gamma$, cell is keratocyte-like [Fig. 2(b) and Movie S2 [39]]. Here the simulated keratocyte-like motion exemplifies how the CF

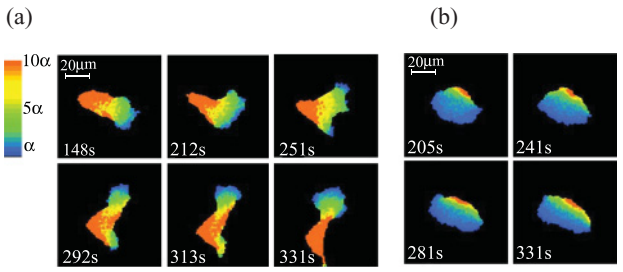


FIG. 2. (Color) Snapshots of the simulated migration in the absence of external guiding signal. (a) Example of amoeba-like motion with $(\alpha_0, \gamma) = (1.4, 4.2)$; and (b) an example of keratocyte-like motion with $(\alpha_0, \gamma) = (7.0, 1.6)$. Concentration of CF is shown with colors.

polarization and the cell motion stabilize each other by forming a feedback loop of the whole cell scale. Realization of different types of migration through modulation of two parameters suggests that the minor modification of reaction rates gives rise to such difference, which is consistent with the observation that an *amiB*-null *Dictyostelium* mutant indeed shows the keratocyte-like movement [41] while the wild-type *Dictyostelium* is a typical amoeba-like cell. In the following, we compare these cell behaviors in different environments.

### B. Superdiffusive migration of amoeboid cells

Spontaneous movement of cells in the absence of external signal provides an important opportunity to examine the quantitative aspects of migration. Plotted in Fig. 3 are the data simulated without external signal for $(\alpha_0,\gamma) = (1.4,4.2)$ (amoeba-like) and $(7.0,1.6)$ (keratocyte-like), which are compared with the observed data of 5.5 hour starved *D. discoideum* wild-type cells [9]. As shown in Fig. 3, the simulated amoeba well fits the observed data, which supports the view that the proposed CF feedback mechanism plays important roles in regulating migration. The simulated keratocyte migration, on the other hand, is largely different from the amoebic data in all panels of Fig. 3.

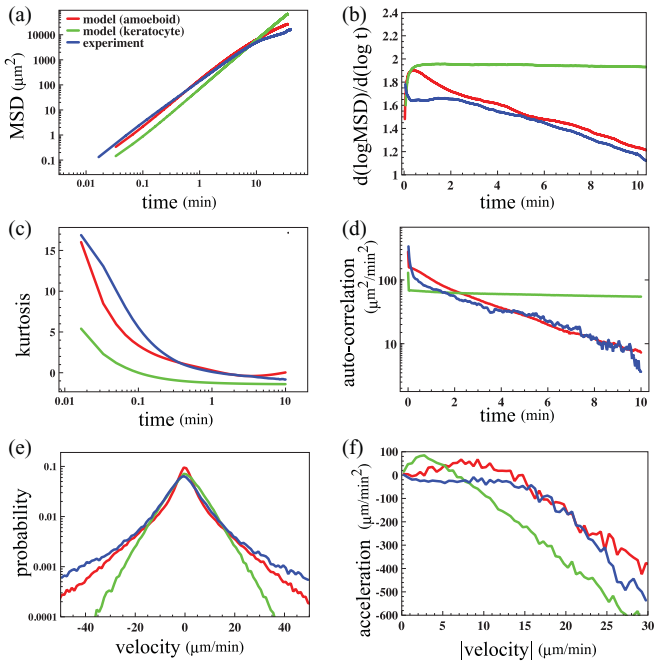


FIG. 3. (Color) Statistical features of trajectories of the center of cell simulated in the absence of guidance signal are compared with the experimental data [9]. Red lines are the simulated amoeba with $(\alpha_0,\gamma) = (1.4,4.2)$, green lines are the simulated keratocyte with $(\alpha_0,\gamma) = (7.0,1.6)$, and blue lines are the experimental data. The simulated data are averaged over 200 trajectories. (a) Log-log plot of mean-square displacement (MSD) as a function of time. (b) Time dependence of the exponent of MSD. (c) Temporal change of kurtosis of the distribution of the position of cell center measured along an arbitrarily chosen direction. (d) Velocity autocorrelation. (e) Distribution of velocity projected onto an arbitrary direction. (f) Relationship between the absolute value of velocity and acceleration projected onto a direction parallel to the velocity.

Shown in Fig. 3(a) is MSD of migration, $\bar{x^2}(t) = \langle[\vec{r}(t) - \vec{r}(0)]^2\rangle$, which can be scaled as $\bar{x^2}(t) \propto t^l$ during $0.05 < t < 5.0$ min, where $\vec{r}(t)$ is the position of the center of cell at time $t$, and the fitted values of the exponent are $l = 1.64$ for the observed data and $l = 1.78$ for the simulated amoeba, both of which significantly differ from the exponent for the Brownian diffusion ($l = 1$) or the ballistic motion ($l = 2$), showing the superdifusive feature during this time scale. Considering the fact that the time scale of the MDCK cell is about two orders of magnitude larger than that of *Dictyostelium*, this feature is comparable with the data of MDCK cell exhibiting $1.5 < l < 1.8$ during $5 < t < 100$ min [8]. In contrast to such superdiffusive migration, the simulated keratocyte shows $l = 1.95$ as expected from the ballistic movement of the observed keratocyte [7]. Temporal variation of the exponent calculated by $l(t) = d[\log \bar{x^2}(t)]/d(\log t)$ is shown in Fig. 3(b). Here $l(t)$ of both the observed and simulated amoebae decreases from $l \approx 1.6$–$1.8$ at $t = 0$ to $l \approx 1.2$–$1.3$ at $t = 10$ min.

As $l(t)$ becomes small, the distribution of position of cells begins to bear a Gaussian feature. Shown in Fig. 3(c) is the kurtosis defined by $\langle[r_a(t) - \langle r_a(t)\rangle]^4\rangle/\langle[r_a(t) - \langle r_a(t)\rangle]^2 - 3$ for the distribution of $r_a(t) = \vec{r}(t)\cdot\vec{e}_a$, where $\vec{e}_a$ is an arbitrarily chosen direction. Kurtosis represents how sharp the peak of the distribution is, and the distribution is Gaussian when the kurtosis is zero. The kurtosis of the simulated and observed amoebae approaches the Gaussian value of 0 at $t \approx 10$ min, suggesting that the motion becomes uncorrelated in the timescale longer than 10 min. Such decay of correlation can be seen in the autocorrelation of velocity of cell: Shown in Fig. 3(d) is $\langle\vec{v}(\tau)\cdot\vec{v}(\tau + t)\rangle_\tau$, where $\vec{v}(t) = d\vec{r}/dt$ and $\langle\dots\rangle_\tau$ is the average taken over both $\tau$ and trajectories. The correlation decays exponentially in both the simulated and observed amoebae with the relaxation time of 3.8 min. These data show that random turns of cell locomotion become uncorrelated in the long-time scale.

The distribution of the amplitude of velocity, however, retains the anomalous non-Gaussian features. As shown in Fig. 3(e), the distribution of $\langle\vec{v}(\tau)\cdot\vec{e}_a\rangle_\tau$ is highly non-Gaussian, decaying more slowly than exponential both in the simulated and observed amoebae. These data imply that the amoeboid motion is persistent more than the simple Gaussian process. The persistent motion of the simulated kerayocyte, on the other hand, shows an exponential distribution with the kurtosis 1.99. The exponential distributions are also found around the peaks for amoeboid cells showing some resemblance to the keratocyte movement for small velocity but with kurtosis 4.22 and 3.24 for the simulated and observed amoebae, respectively.

Features of changing velocity are also nontrivial as clearly seen in the nonlinear relation between velocity and acceleration [Fig. 3(f)]. The negative acceleration or the strength of "brake" is small for amoebae running with small to medium velocity, which is consistent with the data of Fig. 3(e) on the persistency of motion, and is also consistent with the simulated [25] and the observed [42] "inertia-like" features of cell motion.

Thus, the dynamical behaviors of amoeba in Fig. 3 are explained by the inertia-like persistent movement, which is interrupted by the random changing of direction of motion in the time scale of several minutes, and such coupled

processes of persistent motions and random turns bring about the non-Brownian superdiffusive migration as observed for $t < 10$ min. The simulated data well reproduce this dynamics, so the question to be asked is how the CF feedback mechanism generates these dynamical behaviors.

### C. The CF feedback underlies the superdiffusive migration

Shown in Fig. 4(a) is the persistency of migration defined by $p(t_0) = \langle|\vec{r}(0) - \vec{r}(t_0)|/s(0:t_0)\rangle$, where $s(0:t_0)$ is the contour length calculated along the simulated trajectory of $\vec{r}(t)$ from $t = 0$ to $t = t_0$ with $t_0 = 1000$ s. $p(t_0)$ is large in the keratocyte-like regime of large $\alpha_0$ and small $\gamma$, while $p(t_0)$ is small in the regime at which both $\alpha_0$ and $\gamma$ are large or both of them are small. $p(t_0)$ is, on the other hand, at the intermediate level in the amoeboid regime of small $\alpha_0$ and large $\gamma$. This intermediate level of persistency of the simulated amoeba is consistent with its dynamical persistency as shown in Fig. 3.

The intermediate level of persistency should be intrinsically related to the way how the straight motion of amoeba is interrupted: As shown in Fig. 2(a), the simulated amoeba spends typically about 100 s to gradually turn into a new direction. This turning is associated with the change in the cell shape to show the letter "Y"-like transient shape with multiple protruding edges. To examine the correlation between the appearance of such transient shape and the change in moving direction, it is convenient to define the tripole moment of cell shape $A_3$, which is defined by the coefficient of $P_3(\cos\theta)$, the third-order Legendre polynomial, in the multipole expansion of the shape of the cell boundary: Here the shape of the cell boundary is represented as a function of the angle $\theta$ measured around the cell center and is expanded by the Legendre polynomials with its third-order coefficient being used as the characteristic of the "Y"-like shape of the cell boundary. Detailed definition of $A_3$ is given in the Supporting Material [39]. $A_3$ has a large positive value when the leading edge spreads to exhibit a "Y"-like shape and a large negative value when the rear side of cell spreads wider than the leading edge as explained in Fig. S2 [39]. Shown in Fig. 4(b) is the simulated correlation between $|A_3|$ and the turning angle between vectors $\Delta\vec{r}(t) = \vec{r}(t - \Delta t') - \vec{r}(t)$ and $\Delta\vec{r}(t + \Delta t')$ with $\Delta t' = 50$ s. This correlation is largest in the amoeboid regime, showing that the simulated amoeba changes its moving direction by developing the tripole shape.

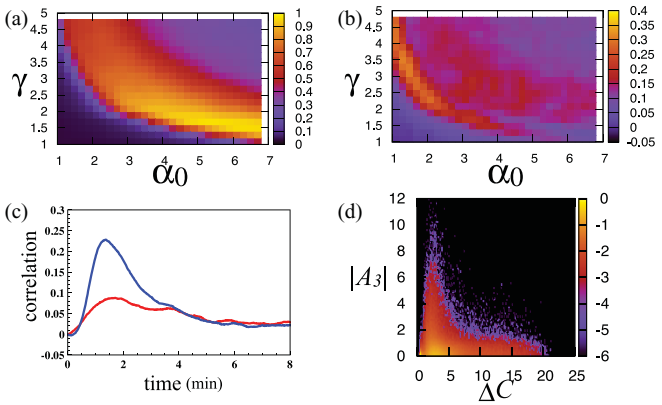


FIG. 4. (Color) Statistical features of locomotion in the absence of external signal. (a) Persistency of motion of the center of cell. (b) Correlation between the tripole moment of cell shape, $|A_3|$, and the angle of changing direction of motion. (c) Correlation between $|A_3|$ and the CF polarization, $\Delta C$, of the amoeba-like cells are shown by $F_{AC}(t)$ (blue line) and $F_{CA}(t)$ (red line). (d) Distribution of $\Delta C(t)$ and $|A_3(t)|$ of the amoeba-like cells. Color represents logarithm of the distribution. In panels c and d, the parameters are $(\alpha_0, \gamma) = (1.4, 4.2)$.

Furthermore, such appearance of the tripole cell shape is intimately related with the loss of CF polarity. Here the CF polarity is measured by $\Delta C(t) = \sigma_c(t)/\bar{C}(t)$, where $\sigma_c(t)$ and $\bar{C}(t)$ are standard deviation and average, respectively, of the CF distribution in each cell. Plotted in Fig. 4(c) is the cross-correlation, $F_{AC}(t) = \langle|A_3(\tau)|\Delta C(\tau + t)\rangle_\tau/(\langle|A_3|\rangle_\tau\langle\Delta C\rangle_\tau)$ and $F_{CA}(t) = F_{AC}(-t)$. At $t \approx 100$ sec, both $F_{AC}(t)$ and $F_{CA}(t)$ have distinct peaks, showing the delay of responses of $\approx 100$ s. Such delayed responses between $|A_3|$ and $\Delta C$ should be due to the time needed for cells to turn as exemplified in Fig. 2(a). We can find that $F_{AC}(0)$ or $F_{CA}(0)$ is almost 0, which implies that $\Delta C$ and $|A_3|$ are anticorrelated at the same instance. This anticorrelation, or the concurrency of the cell shape deformation and the loss of CF polarity, can be clearly seen in the two-dimensional distribution pattern of $\Delta C$ and $|A_3|$ as plotted in Fig. 4(d). This distribution shows that there are two states in locomotion, the persistent state with small $|A_3|$ and large $\Delta C$, and the turning state with large $|A_3|$ and small $\Delta C$. In this way the superdiffusive migration is described by a switchlike dynamics between these states with the typical switching timescale of around 100 s.

### D. Efficiency of migration

Migrating cells such as *D. discoideum* and keratocytes show chemotaxis when the chemical signal distributes nonuniformly around them. When obstacles prevent cells from straightforwardly following the chemical gradient, however, cells may have to employ some trial-and-error strategy to go around the obstacles to reach the goal at which the chemical signal is highly concentrated. Motion of the cell in a maze corridor has been simulated to show that the zig-zag motion of cell facilitates escape from the maze [21]. From the argument of the previous subsections in this paper, we expect that the superdiffusive motion of amoeboid cells should help chemotaxis in such complex situations: The cell may use the switching behavior underlying the superdiffusive motion for the efficient trial-and-error finding of the route. In this subsection we test this hypothesis by comparing two different types of motion, amoeba- and kertocyte-like locomotion.

We first show that the persistent motion of keratocyte is most efficient to reach the target when the environment around cell is simple enough to allow the straight motion. Shown in Fig. 5(a) is the efficiency defined by the distance how far the cell can travel along the gradient of the concentration of the signal chemoattractant. Here the signal is distributed along the $y$ direction as $S_j = \exp[-y_j/(100\mu\text{m})]$. Among various modes of motion simulated in the present model, keratocyte has the highest efficiency as expected.

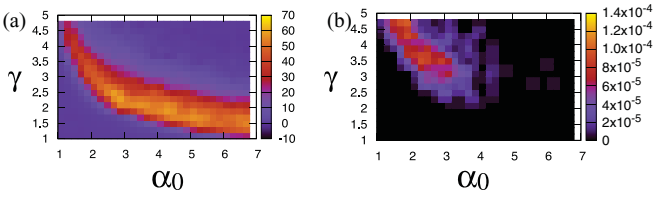


FIG. 5. (Color) Efficiency of migration. (a) Efficiency for responding the signal having the simple gradient along the $y$ direction. The efficiency is defined by $\langle y(t_0) - y(0)\rangle$ with $t_0 = 1000$ s, where $y(t)$ is the $y$ coordinate of the position of the center of cell at time $t$. (b) Efficiency for the mazelike environment. The efficiency is defined by $\langle 1/T\rangle$, where $T$ is the time needed for cell to reach the target, i.e., the source of the chemoattractant.

The keratocyte migration, however, becomes inefficient when the environment is complex to prevent cells from moving straightforwardly. Eukaryotic cells *in vivo* often move in such a complex environment, which may consist of obstacles such as tissue cells or extracellular matrices. Leukocytes in animal bodies, for example, migrate through a web of collagen fibers [43–45], so that those cells sometimes go against the chemoattractant gradient to find a detour to approach the target. To explore the efficiency in such complex environment, we here consider a two-dimensional $xy$ plane on which obstacles are arranged in a mazelike manner.

We prepare the membrane walls through which a cell does not pass: The system is surrounded by a large square wall inside of which a horizontal ($x$-directional) wall and a vertical ($y$-directional) wall are arranged as shown in Fig. 6, which merge to form a letter "T"-like obstacle. The signal chemoattractant does not permeate through these walls except a left part of the horizontal wall, which is colored red in Fig. 6. In a right part of the horizontal wall, there is a doorway through which both signal and cell can pass. A source of signal is placed on the plane across the obstacle from the initial position of cell. The distribution of $S_j$ is determined by solving the Laplace equation, $\Delta S(\vec{r}) = -M\delta(\vec{r} - \vec{r}_s)$ with the boundary condition $S(\vec{r}) = 0$ at the the wall surrounding the system, where $\vec{r}_s$ is the position of the signal source. Further explanation of the Laplace equation is given in the Supporting Material [39].

Shown in Fig. 6 are snapshots of amoebic cell motion. Since the signal permeates through the red "window" located near the initial position of the cell, the cell is attracted to the window. This attractive motion is induced through the CF feedback with CF accumulated at the rear of cell (40–55 s). However, the cell can not pass through the window, and hence the cell is trapped there. It should be noted that the halted centroid motion upon collision of the cell against the wall does not completely stop the retrograde flow of CF, but in the simulated cell, the CF pattern continues to change due to the continuous deformation of the cell while being trapped to the window. The retrograde flow of CF, however, is weakened due to this trapping, and the direction of the flow is largely changed. This marked decrease and alteration of direction of the flow is consistent with the observed behavior of the actin flow in cells colliding against the obstacle [36]. Accumulation of CF at the rear of cell is ceased in this way, and CF begins to spread toward the front (95 s), which gives rise to the motion

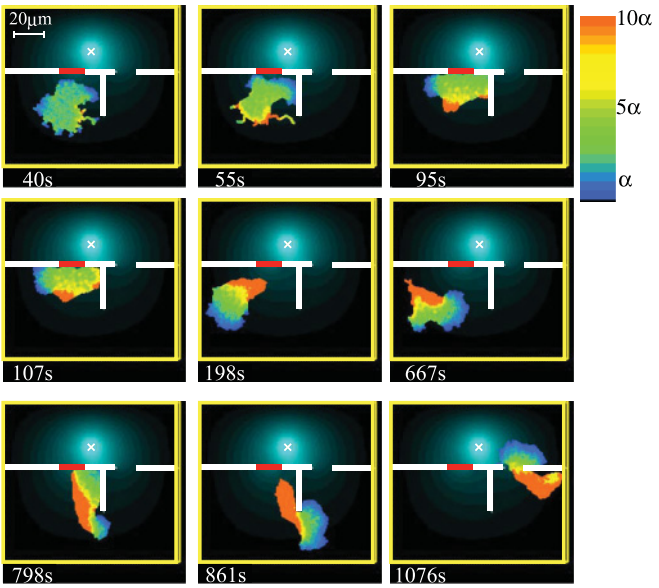


FIG. 6. (Color) Snapshots of cell movement in the maze-like environment simulated with $(\alpha_0, \gamma) = (2.0, 4.2)$. Concentration of cortical factor normalized by $3\alpha$ is shown in color. A bar at the left top panel shows the length of 20 $\mu$m. The number at the left bottom in each panel is time lapse. A red colored line is the window in the wall, through which the extracellular chemical signal permeates but the cell does not pass. A light blue pattern indicates the extracellular chemical signal secreted from the point at a white cross. The cell is surrounded by the rectangular walls, the outside of which is thought of as a "sink" of the chemical signal. Within the rectangle, the horizontal and vertical walls prevent the cell from moving toward the signal source.

"repelled" from the wall (107–198 s). The cell once left the wall is still attracted by the signal and can come back to be trapped again (667 s), but after a protruding edge happens to go over the vertical wall (798 s), that edge is elongated through the CF feedback effect by sensing the signal gradient coming from the doorway (864 s) and finally finds the doorway to reach the signal source (1076 s). In this way, it is apparent that the localized work of CF feedback is vital to leave the trap and to find a detour by elongating a searching tip of cell. See also Movie S3 [39] for the cell locomotion to solve the maze problem.

Strategy of cells to solve the maze problem can be quantified by defining the efficiency as the averaged inverse of time necessary for the cell to reach the source. As shown in Fig. 5(b), the strategy is most efficient in the amoeboid regime of small $\alpha_0$ and large $\gamma$. This most efficient strategy is based on the same mechanism to generate the random turns in the superdiffusive migration: Shown in Fig. 7(a) are the temporal changes of $\langle|A_3(t)|\rangle$ and $\langle\Delta C(t)\rangle$, in which $t = 0$ is the first time instance when the amoeba cell collides against the horizontal wall. After the collision, the cell quickly takes a tripole shape. When the cell goes through this transient tripole shape and begins to leave the wall, which is about 100 s after the collision, the CF polarity is enhanced strongly to drive the cell into a direction to leave the wall. $\langle\Delta C(t)\rangle$ shows a peak at $t \approx 200$ s when the motion to leave the wall is most stable. The distribution pattern in Fig. 7(b) shows that $|A_3(t)|$ and $\Delta C(t)$ anticorrelate

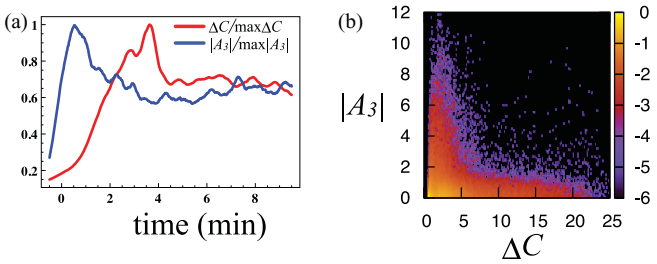


FIG. 7. (Color) Relations between the tripole moment, $|A_3|$, and the CF polarization, $\Delta C$, of amoeba-like cells in the the maze-like environment. (a) Temporal change of $\langle|A_3(t)|\rangle$ (blue line) and $\langle\Delta C(t)\rangle$ (red line). The cell collides against the wall at $t = 0$. Average was taken over 200 trajectories. (b) The distribution of $|A_3|$ and $\Delta C$ at the same instance. Color represents logarithm of the distribution. $(\alpha_0, \gamma) = (2.0, 4.2)$ is used in panels a and b.

as was found in Fig. 4(d). See Fig. 4 and Figs. S3 and S4 [39] to confirm that the relations between $|A_3(t)|$ and changes in moving direction are almost same in simple and complex environments.

In this way the cell shape deformation and the loss of CF polarity concurrently take place in a cell colliding against the wall. The loss of CF polarity erases the memory of motion toward the wall and gives rise to a tripole cell shape to change the moving direction. This is the same mechanism of how the persistent migrations is interrupted by fluctuation in the simple environment. Thus, the switchlike dynamics between the persistent state and the turning state, which is a source of the superdiffusive motion in the simple environment, is a driving force for the efficient route finding in the complex environment.

## III. DISCUSSION

In this paper the observed non-Brownian dynamics of amoeboid migration was explained by the slow whole-cell scale feedback dynamics of inhibitory factor of actin polymerization. Thus generated positive feedback stabilizes the persistent migration, but the fluctuation of cell shape interrupts this motion to turn the cell into a different direction. Switching behaviors between persistent motions and random turns are the source of the observed superdiffusive migration of amoeba-like cells and also drive cells to find a detour in the complex environment. The model is developed so as to focus on the proposed feedback mechanism and does not treat the force-velocity relations and signaling pathways explicitly. This implicit treatment of important processes should limit the ability of the model to describe the short-time-scale dynamics, and hence for more quantitative description, the multiscale modeling is necessary to integrate these fast processes and the slow CF dynamics highlighted in the present model. Also important is to improve the model to take account of effects of the advective actin flow observed in the substrate-fixed frame. Such flow should be determined by the balance among the rate of actin network polymerization, the amplitude of cell shape deformation, and the efficiency of adhesion of cell to the substratum [31], and it should be intriguing to examine whether this advective flow helps cells to solve the maze problem.

Even with the present coarse-grained model, however, it should be meaningful to quantitatively check the proposed hypothesis that the same mechanism, the CF feedback mechanism, works in both simple and complex environments. For the maze-solving behaviors, predictions made with the present model on the redistribution of CF and those on the development of tripole cell shape can be quantitatively compared with the experimental observations when the micrometer-scale fabrication technique [42] is applied to the construction of the maze-like environment. In particular, when the deficiency of genes relevant to cellular motility should be systematically examined, it would be possible to directly compare the phase diagrams on the $(\alpha_0, \gamma)$ plane with the experimental data. In a recent paper of Ambravaneswaran *et al.*, the chemotactic crawling of a neutrophil cell in a channel which bifurcates into two symmetric or asymmetric channels has been reported [46]. This experimental setup has offered the opportunity to examine the relation between the cell shape fluctuation and the cell decision of its moving direction, so that the quantitative comparison with such data and the simulated results with the present model should be important.

The amoeboid strategy should be also examined quantitatively with the single-cell tracking experiment in animal bodies. In animal bodies, we can expect that the amoeboid strategy is efficient to circumvent other cells or extracellular matrices, and indeed, random-walk-like behaviors with the persistent migration and its interruption have been observed in migrating interneurons within the developing cerebral cortex [47]. Further quantitative comparison between simulations and observations in animal bodies should be important.

The present simulation showed that the amoeboid strategy is the most "intelligent" strategy to solve the maze problem. Keratocyte-like cells move more persistently, but the infrequent turnings make the strategy less efficient in complex environment. Thus, the way the persistent motion and the interruption of the persistent motion are combined is a key to the efficient strategy, and the amoeboid strategy is a method for the proper combination, though the method inevitably generates the randomly fluctuating superdiffusive motion in the absence of an external signal. Other organisms such as *Escherichia coli* or *Paramecium caudatum* also use strategies based on fluctuating motion. Although molecular and physical bases for those strategies are quite different from those of the amoeboid strategy, it would be interesting to compare their statistical features such as efficiency and persistency of motion to the data of the present paper to explore the general principle of strategies that microorganisms take in complex environments.

## ACKNOWLEDGMENTS

We thank Dr. T. Takagi of Nara Medical University and Dr. M. J. Sato of Osaka University for providing their experimental data and important comments. We also thank Prof. H. Nishimori of Hiroshima University for his useful comments. This work is in part supported by the Global COE Program G14 (Formation and Development of Mathematical Sciences Based on Modeling and Analysis) of the Ministry of Education, Culture, Sports Science and Technology of Japan.

[1] J. A. Cooper and D. A. Schafer, Curr. Opn. Cell. Biol. **12**, 97 (2000).
[2] T. D. Pollard and G. G. Borisy, Cell **112**, 453 (2003).
[3] J. V. Small and G. P. Resch, Curr. Opin. Cell. Biol. **17**, 517 (2005).
[4] D. Bray and J. G. White, Science **239**, 883 (1988).
[5] P. Vallotton, S. L. Gupton, C. M. Waterman-Storer, and G. Danuser, Proc. Natl. Acad. Sci. USA **101**, 9660 (2004).
[6] C. A. Wilson, M. A. Tsuchida, G. M. Allen, E. L. Barnhart, K. T. Applegate, P. T. Yam, L. Ji, K. Keren, G. Danuser, and J. A. Theriot, Nature (London) **465**, 373 (2010).
[7] K. Keren, Z. Pincus, G. M. Allen, E. L. Barnhart, A. Mogilner, and J. A. Theriot, Nature (London) **453**, 475 (2008).
[8] P. Dieterich, R. Klages, R. Preuss, and A. Schwab, Proc. Natl. Acad. Sci. USA **105**, 459 (2008).
[9] H. Takagi, M. J. Sato, T. Yanagida, and M. Ueda, PLoS ONE **3**, e2648 (2008).
[10] T. D. Yang, J.-S. Park, Y. Choi, W. Choi, T.-W. Ko, and K. J. Lee, PLoS ONE **6**, e20255 (2011).
[11] M. Herant and M. Dembo, Biophys. J. **98**, 1408 (2010).
[12] A. F. M. Marée, A. Jikine, A. Dawes, V. A. Grieneisen, and L. Edelstein-Keshet, Bull. Math. Biol. **68**, 1169 (2006).
[13] E. L. Barnhart, K.-L. Lee, K. Karen, A. Mogilner, and J. A. Theriot, PLoS Biol. **9**, e1001059 (2011).
[14] C. L. Manahan, P. A. Iglesias, Y. Long, and P. N. Devreotes, Ann. Rev. Cell. Dev. Biol. **20**, 223 (2004).
[15] A. Levchenko and P. A. Iglesias, Biophys. J. **82**, 50 (2002).
[16] Y. Xiong, C.-H. Huang, P. A. Iglesias, and P. N. Devreotes, Proc. Natl. Acad. Sci. USA **107**, 17079 (2010).
[17] H. Levine, D. A. Kessler, and W.-J. Rappel, Proc. Natl. Acad. Sci. USA **103**, 9761 (2006).
[18] I. Hecht, M. L. Skoge, P. G. Charest, E. Ben-Jacob, R. A. Firtel, W. F. Loomis, H. Levine, and W.-J. Rappel, PLoS Comput. Biol. **7**, e1002044 (2011).
[19] A. Gamba, A. de Candia, S. D. Talia, A. Coniglio, F. Bussolino, and G. Serini, Proc. Natl. Acad. Sci. USA **102**, 16927 (2005).
[20] M. Onsum and C. V. Rao, PLoS Comput. Biol. **3**, e36 (2007).
[21] I. Hecht, H. Levine, W.-J. Rappel, and E. Ben-Jacob, PLoS ONE **6**, e21955 (2011).
[22] M. P. Neilson, D. M. Veltman, P. J. M. van Haastert, S. D. Webb, J. A. Mackenzie, and R. H. Insall, PLoS Biol. **9**, e1000618 (2011).
[23] S. I. Nishimura, M. Ueda, and M. Sasai, PLoS Comput. Biol. **5**, e1000310 (2009).
[24] S. I. Nishimura and M. Sasai, J. Theor. Biol. **245**, 230 (2007).
[25] S. I. Nishimura and M. Sasai, Phys. Rev. E **E71**, 010902 (2005).
[26] R. W. Washington and D. A. Knecht, BMC Cell Biol. **9**, 10 (2008).
[27] D. Cox, J. Condeelis, D. Wessels, D. Soll, H. Kern, and D. A. Knech, J. Cell Biol. **116**, 943 (1992).
[28] J. Faix, H. Steinmetz, M. Boves, R. A. Kammerer, F. Lottspeich, U. Mintert, J. Murphy, A. Stock, U. Aebi, and G. Gerisch, Cell **86**, 631 (1996).
[29] Y. Wu, M. O. Hannigan, A. Kotlyarov, M. Gaestel, D. Wu, and C.-K. Huang, Biochem. Biophys. Res. Comm. **316**, 666 (2004).
[30] D. Wessels, D. F. Lusche, S. Kuhl, P. Heid, and D. R. Soll, J. Cell Sci. **120**, 2517 (2007).
[31] L. B. Smilenov, A. Mikhailnov, R. J. Pelham Jr., E. E. Marcantonio, and G. G. Gundersen, Science **286**, 1172 (1999).
[32] M. Vincente-Manzanares, C. K. Choi, and A. R. Horwitz, J. Cell Sci. **122**, 199 (2009).
[33] A. Y. Alexandrova, K. Arnold, S. Schaub, J. M. Vasiliev, J. J. Meister, A. D. Bershadsky, and A. B. Verkhovsky, PLoS ONE **3**, e3234 (2008).
[34] W. Shih and S. Yamada, Biophys. J. **98**, L29 (2010).
[35] H. A. Benink and C. A. Mandato, Mol. Biol. Cell **11**, 2553 (2000).
[36] P. Vallotton, G. Danuser, S. Bohnet, J.-J. Meister, and A. B. Verkhovsky, Mol. Biol. Cell **16**, 1223 (2005).
[37] Y. Fukui, Cell Biol. Int. **26**, 933 (2002).
[38] P. G. Charest and R. A. Firtel, Curr. Opin. Gen. Dev. **16**, 339 (2006).
[39] See Supplemental Material at http://link.aps.org/supplemental/10.1103/PhysRevE.85.041909 for supporting text, figures, table, and movies.
[40] P. J. van Haastert, J. Cell Biol. **96**, 1559 (1983).
[41] Y. Asano, T. Mizuno, T. Kon, A. Nagasaki, K. Sutoh, and T. Q. P. Uyeda, Cell. Motil. Cytoskel. **59**, 17 (2004).
[42] N. L. Jeon, H. Baskaran, S. K. W. Dertinger, G. M. Whitesides, L. V. D. Water, and M. Toner, Nat. Biotech. **20**, 826 (2002).
[43] P. Friedl, S. Borgmann, and E.-B. Bröcker, J. Leukoc. Biol. **70**, 491 (2001).
[44] K. Wolf, R. Muller, S. Borgmann, E. Brocker, and P. Friedl, Blood **102**, 3262 (2003).
[45] A. Pathak and S. Kumar, Integr. Biol. **3**, 267 (2011).
[46] V. Ambravaneswaran, I. Y. Wong, A. J. Aranyosi, M. Toner, and D. Irimia, Integr. Biol. **2**, 639 (2010).
[47] D. H. Tanaka, M. Yanagida, Y. Zhu, S. Mikami, T. Nagasawa, J. Miyazaki, Y. Yanagawa, K. Obata, and F. Murakami, J. Neurosci. **29**, 1300 (2009).